Current Opinion in Solid State and Materials Science 19 (2015) 149–159

Contents lists available at ScienceDirect

Current Opinion in Solid State and Materials Science

journal homepage: www.elsevier.com/locate/cossms

Mechanics for stretchable sensors

Nanshu Lu *, Shixuan Yang

Center for Mechanics of Solids, Structures and Materials, Department of Aerospace Engineering and Engineering Mechanics, Center for Nanomanufacturing Systems for Mobile Computing and Mobile Energy Technologies (NASCENT), Texas Materials Institute, The University of Texas at Austin, Austin, TX 78712, USA

ARTICLE INFO

Article history:
Received 15 October 2014
Revised 5 December 2014
Accepted 14 December 2014
Available online 14 January 2015

Keywords:
Stretchable
Island
Serpentine
Thin film
Polymer substrate

ABSTRACT

In the past decade, high performance stretchable sensors have found many exciting applications including epidermal and *in vivo* monitors, minimally invasive surgical tools, as well as deployable structure health monitors (SHM). Although wafer based electronics are known to be rigid and planar, recent advances in manufacture and mechanics have made intrinsically stiff and brittle inorganic electronic materials stretchable and compliant. This review article summarizes the most recent mechanics studies on stretchable sensors composed of ceramic and metallic functional materials. The discussion will focus around the most popular "island plus serpentine" design where active electronic or sensing components are housed on an array of isolated, micro-scale islands which are interconnected by electrically conductive, stretchable, serpentine thin films. The mechanics of polymer supported islands, freestanding serpentines, and polymer supported serpentines will be introduced. The effects of feature geometry and polymer substrate on the stretchability, compliance, as well as functionality of the sensor system will be discussed in details. The tradeoff between mechanics and functionality gives rise to the challenge of simultaneously optimizing the structure and performance of stretchable sensors.

1. Introduction

Research on flexible electronics started almost 20 years ago [1,2] with the demand of macroelectronics [3], such as paperlike displays [4,5]. Organic semiconductors and conducting polymers were appealing materials for large-area electronics attributing to their intrinsic flexibility, light weight, and low fabrication cost in roll-to-roll processes [6,7]. The other branch of flexible and even stretchable electronics based on high-quality inorganic semiconductors started to emerge in the mid-2000s [8,9]. Inorganic semiconductors exhibit high carrier mobility and excellent chemical stability [8]. Natural abundance and well-established manufacturing processes make them even more appealing. Their intrinsic stiffness and brittleness, however, greatly hindered their application in flexible electronics. Mechanics of stiff/brittle membranes integrated with deformable polymeric substrates have offered insights and solutions to overcome the intrinsic limitations of these materials.

For example, bendable and foldable inorganic electronics including integrated circuits [10,11], solar cells [12], light emitting diodes [13], thin film battery [14], and bio-integrated nanogenerator [15] have been successfully developed by placing fragile materials along the neutral axis of a multilayer stack. Neutral axis is defined as the line (or the plane for 3D problems) whose strain remains zero when the system is under pure bending. Using Euler–Bernoulli beam theory [16], the position of the neutral axis of an n-layer laminate can be determined by the following equation [10].

$$b = \frac{\sum_{i=1}^{n} \bar{E}_i h_i \left[\left(\sum_{j=1}^{i} h_j \right) - \frac{h_i}{2} \right]}{\sum_{i=1}^{n} \bar{E}_i h_i}, \tag{1}$$

where b denotes the distance between the top surface of the laminate to the neutral axis, $i = 1$ represents the top layer, $\bar{E}_i = E_i/(1 - \nu_i^2)$ is the plane strain Young's modulus with ν_i being the Poisson's ratio of the ith layer, and h_i represents the thickness. Bending-induced strain can be calculated analytically using:

$$\varepsilon = \frac{y}{\rho}, \tag{2}$$

where ρ represents the radius of the neutral axis and y is the distance from the neutral axis to the point of interest. Therefore, when the median plane of a brittle layer of thickness h is aligned with the neutral axis, the maximum bending induced tensile strain in this brittle layer can be calculated by substituting $y = h/2$ in Eq. (2), which indicates that even when the brittle layer is placed along the neutral axis, the maximum strain is still proportional to the thickness of this brittle layer. However, we have to be careful when

* Corresponding author. Tel.: +1 512 471 4208.
E-mail address: nanshulu@utexas.edu (N. Lu).

http://dx.doi.org/10.1016/j.cossms.2014.12.007
1359-0286/

using Eqs. (1) and (2) because they are only applicable to a laminate with small elastic mismatch between different layers. With flexible photonic strain sensors [17], we find that the Euler–Bernoulli beam theory breaks down when a soft layer is sandwiched between two stiff layers because significant shear can develop in the soft layer, leading to the so called "split of neutral axis", i.e. multiple neutral axes can appear within one multilayer laminate. This finding breaks the limit of conventional flexible electronics where all the brittle materials have to be placed along one neutral plane. Instead, it suggests a possibility to build flexible electronics with multiple layers of active components because of the presence of multiple neutral axes.

Compared with flexible electronics, the mechanics for stretchable electronics are more complicated. An earlier strategy to achieve stretchable circuits is to harness the wrinkling (i.e., no delamination between film and substrate) and buckling delamination of stiff nanoribbons or nanomembranes on soft elastomeric substrates [10,18–25]. The controlled wrinkle formation of stiff membranes on elastomeric substrates dated back to late 90s [26–28]. Wrinkled conductors were later found to be useful as stretchable interconnects [22–25]. Wrinkled semiconductor nanoribbons were first realized in 2006 [18,19]. While some analysis on the critical membrane force to initiate wrinkle [29] and buckling delamination [30–32] were even earlier than above experiments, these experiments have stimulated numerous mechanics studies to predict the wavelength and amplitude of the wrinkled patterns [33–45].

Due to difficulties associated with the fabrication, encapsulation, and bio-integration of wrinkled or buckled circuits, a new mechanics strategy to build stretchable electronics, the "island plus serpentine" design [46], became more popular. The idea is simple: instead of using continuous nanomembranes or straight nanoribbons, inorganic materials can be patterned into isolated microislands and serpentine-shaped meandering ribbons. As the Young's moduli of elastomers are four to six orders lower than inorganic semiconductors, when the elastomer substrate is stretched, it cannot generate large enough stress to be transferred to the stiff islands which are bonded to the elastomer. Therefore strains in the islands remain very small and the brittle materials housed on the islands can stay intact even under very large applied strains to the substrate. To complete the circuits, isolated islands have to be interconnected by extremely stretchable conductors. While straight thin metal films well adhered to polyimide substrate have demonstrated stretchability up to 50% [47–49], the deformation is enabled by plastic mechanism, which is not reversible. One way to enable reversible resistance of straight thin metal film with applied loading and unloading is through a microcrack facilitated mechanism [50], but their fatigue behavior could be a concern. Wrinkled stretchable interconnects have been studied extensively [23–25] but they are difficult to encapsulate and are easy to fracture even under very slight over stretch. Buckled, encapsulated interconnects have successfully linked the isolated islands to complete the circuits [10,51–53] but the fabrication requires transfer printing circuits on pre-stretched elastomer and the buckled interconnect bridges make it difficult to integrate the device with other surfaces. In-plane, serpentine-shaped interconnects can get rid of both troubles – they can be transfer printed onto relaxed elastomers and as fabricated sensors have a flat surface which is easy to encapsulate or to integrate. Serpentines are stretchable because they are like in-plane springs, which can achieve large end-to-end displacement through geometric reconfiguration instead of straining the interatomic distance of the material [54,55]. What's more convenient is that the geometric reconfiguration can be highly reversible due to the small induced strains.

The "island plus serpentine" strategy and its more stretchable variation, the "filamentary serpentine" network, have enabled an explosion of stretchable electronics [56,57] in the late 2000s when the concept of bio-integrated electronics was proposed. So far, bio-integrated electronics has demonstrated exciting applications including epidermal electronic systems (EES) for vital sign monitoring and human machine interface [58–64] (Fig. 1A), conformal epicardial mapping/treatment sheet [65] (Fig. 1B) or sock [66], and instrumented balloon catheter for minimally invasive surgery [67] (Fig. 1C). More detailed materials and mechanics strategies for bio-integrated electronics have been summarized in several recent review articles [68–73]. In addition to bio-integrated electronics, stretchable sensors based on freestanding "island-plus-serpentine" network (i.e., not bonded to polymer substrates) have also found use in structure health monitors (SHM) for their extreme extensibility so that microfabricated, wafer sized sensor network can be deployed hundreds of times to cove huge civil or aerospace structures [74,75] (Fig. 1D). As bending eventually induces tensile strains on the surface of the structure, the "island-plus-serpentine" structure has also enhanced the bending and folding capability of silicon electronics integrated on stiff substrates (e.g., Kapton, printing papers, fabrics, etc.) through a soft strain isolation interlayer [76,77].

This review will summarize some recent studies of the fundamental mechanics of polymer-supported stiff islands and serpentines either freestanding or bonded to polymer substrates. The tradeoff between mechanics and functionality will also be discussed and some optimization strategies will be offered. This review is organized as follows: Section 2 will focus on the mechanics of polymer-supported stiff islands. Section 3 will investigate freestanding and polymer-supported serpentine, respectively. Concluding remarks will be given in Section 4.

2. Stretchable islands on polymer substrates

Mechanics of stiff islands on polymer substrate is important to not only the mechanical reliability of the stretchable device, but also the functionality of the electronics and sensors. In terms of mechanical reliability, failure modes such as channel cracking in ceramic islands [78] and island/substrate delamination [79] are commonly seen. In terms of functionality, semiconductor mobility [80,81] and strain gauge gauge factor [58,64,65,82,83] can be greatly affected by the strain transferred from substrates to islands. In this section, we will use stretchable strain gauges made of piezoresistive silicon strips bonded on polymer substrates (Fig. 1B) as an example to illustrate the tradeoff between mechanics and functionality.

Strain gauges are widely applied to measure mechanical deformation of structures and specimens. Stretchable strain gauges offer unique capability of measuring large strains in soft materials and bio-tissues. While metallic foil gauges usually have a gauge factor slightly over 2 [84], single crystalline silicon demonstrates intrinsic gauge factors as high as 200 due to their piezoresistive property [85–87]. Although silicon is an intrinsically stiff and brittle material, flexible and even stretchable strain gauges have been achieved by integrating thin silicon strips on soft and deformable polymer substrates [64,65,83]. Compared with polymer based stretchable strain gauges [88,89], silicon based ones exhibit less drift, better reversibility, and faster time response. But depending on the substrate material, the behaviors of silicon strain gauges are very different: their gauge factors spanned from 0.23 [64,65] to 43 [83] and stretchability from less than 1% [83] to more than 25% [64,65].

To achieve a fundamental understanding of the large variation in gauge factor and stretchability of reported flexible/stretchable silicon-on-polymer strain gauges, 2D plane strain finite element models (FEM) and semi-analytical models are established to reveal the effects of the length of the silicon strip, and the thickness and

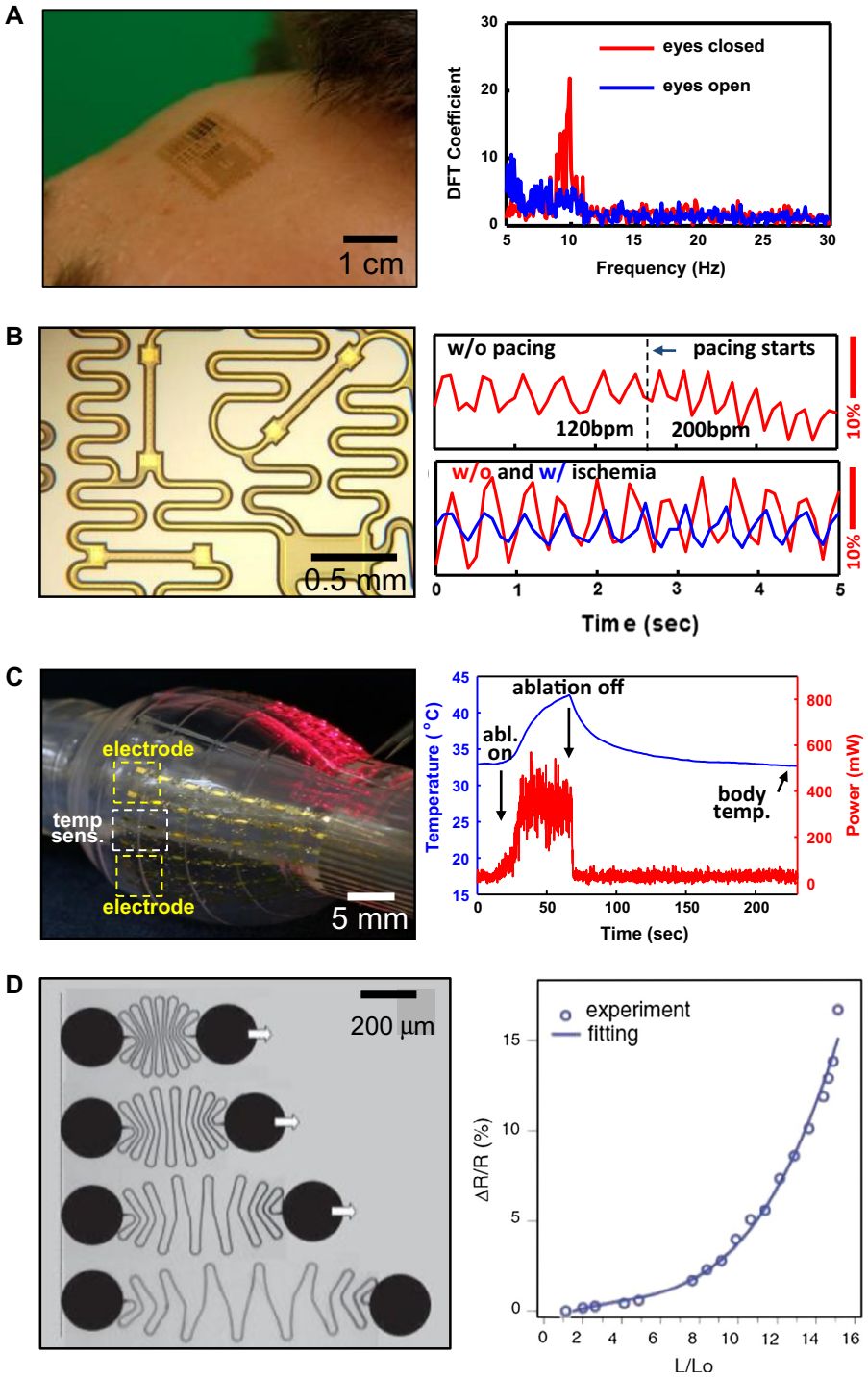

Fig. 1. Examples of stretchable sensors. (A) Epidermal electronic system integrated on human forehead for the measurement of brain signal [58]. (B) Epicardial stretchable strain gauges picking up heart beat amplitude and frequency [65]. (C) Instrumented inflatable balloon catheter delivering *in vivo* radio frequency (RF) ablation to rabbit heart with *in situ* temperature characterization [67]. (D) Utmost expandable SHM sensors based on freestanding serpentines with very long arms [75].

modulus of the polymer substrate (Fig. 2) [82]. A 3D silicon island on polymer substrate problem shown in Fig. 2A is simplified into a 2D plane strain problem as depicted in Fig. 2B. We use L to represent the length of the silicon strip, h and H the thicknesses of silicon and polymer, respectively. To minimize the number of variables, the size of the unit cell is fixed to be $1.5L$ for all the models following a convention of island-on-polymer analysis [77,90,91]. While the average strain ε_{avg} in silicon reflects the gauge factor (GF), the maximum strain in silicon ε_{max} governs the stretchability of the system. Through dimensional analysis, we have determined three dimensionless variables:

$$\frac{\varepsilon_{avg}}{\varepsilon_{app}} = f\left(\frac{\overline{E}_{Si}}{\overline{E}_s}, \frac{L}{h}, \frac{h}{H}\right), \tag{3}$$

and

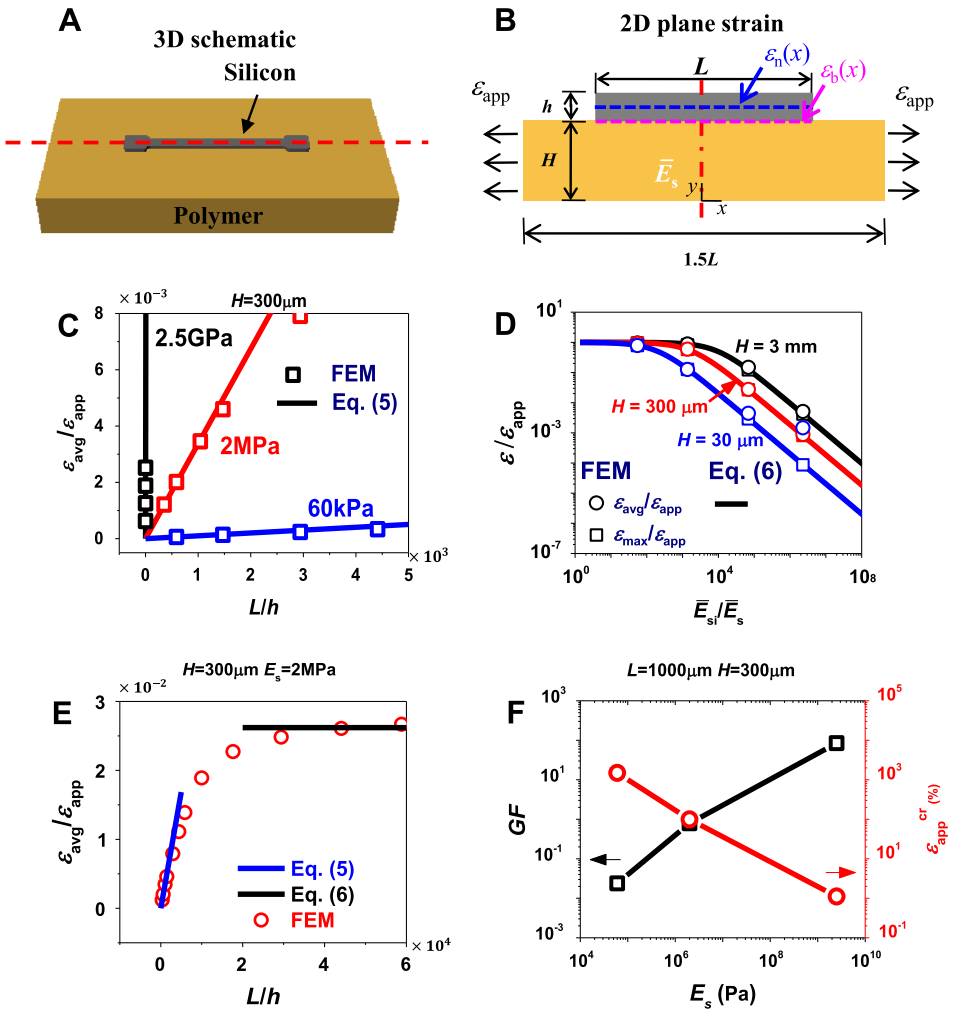

Fig. 2. Strain analysis of stiff island on polymer substrate [82]. (A) A 3D schematic of silicon strip on polymer substrate. (B) The 2D plane strain model of A. (C) When $L/H \ll 1$, Eq. (5) captures the linear relation between strain and substrate modulus as well as island size. (D) When $L/H \gg 1$, Eq. (6) can well predict the average and maxim strains in the island. (E) Semi-analytical solutions given by Eqs. (5) and (6) can capture strains for extremely short or long islands, but not islands with mediocre length. (F) The universal tradeoff between *GF* and stretchability.

$$\frac{\varepsilon_{max}}{\varepsilon_{app}} = g\left(\frac{\bar{E}_{Si}}{\bar{E}_s}, \frac{L}{h}, \frac{h}{H}\right), \tag{4}$$

where the substrate "Si" denotes silicon and "s" represents substrate. Our goal is to find out the functional forms of f and g. Several shear lag models have been built to solve similar problems of stiff thin films on compliant substrates [65,92,93], but all of them had to make special assumptions of the shear stress distribution along the film/substrate interface, none of which is generic enough to be applicable to wide ranges of $\bar{E}_{Si}/\bar{E}_s$, L/h, and H/h. As a result, we will first use FEM to find exact solutions for $\varepsilon_{avg}/\varepsilon_{app}$ and $\varepsilon_{max}/\varepsilon_{app}$ over wide ranges of all three variables, and then use analytical methods to derive the f and g functions for extreme cases (e.g. $L/H \gg 1$ and $L/H \ll 1$).

When $L/H \ll 1$, $h/H \ll 1$ is also true since experimentally $L > h$ is always valid. In this case, the substrate can be considered infinitely thick and H is no longer a relevant variable in this problem. Therefore ε_{avg} and ε_{max} only depend on $\bar{E}_{Si}/\bar{E}_s$ and L/h. Through free body diagram and equilibrium analysis of the silicon strip [82], we find out that

$$\frac{\varepsilon}{\varepsilon_{app}} = \alpha \frac{\bar{E}_s}{\bar{E}_{Si}} \frac{L}{h}, \tag{5}$$

where α is a proportional coefficient to be determined through fitting FEM results of small L's and is a generic coefficient which once fitted, should be applicable to all combinations of L, H, and E_s, provided $L/H \ll 1$. α is found to be 0.219 for $\varepsilon_{avg}/\varepsilon_{app}$ and 0.279 for $\varepsilon_{max}/\varepsilon_{app}$. We then plot Eq. (5) against FEM results of all the other combinations of E_s and H and it turns out that Eq. (5) is able to capture very wide ranges of E_s when $L/H \ll 1$, for both $\varepsilon_{avg}/\varepsilon_{app}$ (Fig. 2C) and $\varepsilon_{max}/\varepsilon_{app}$ (not shown). In summary, when $L/H \ll 1$, the average and maximum strains in silicon scale linearly with $\bar{E}_s$ and L, i.e., the stiffer substrate and the longer island (compared to the thickness of the island) yield higher strains in the island. Since $\bar{E}_s$ can be easily changed by orders of magnitude, e.g., from 2.5 GPa for Kapton and polyethylene terephthalate (PET) to 60 kPa for Ecoflex [58], strains in silicon can be tuned across orders of magnitude too.

When $L/H \gg 1$, assuming $L/h \gg 1$ is always valid, relevant variables reduce to $\bar{E}_{Si}/\bar{E}_s$ and h/H. Through decomposed tension and bending boundary conditions [82], we have derived

$$\frac{\varepsilon}{\varepsilon_{app}} = \frac{1}{1 + a\frac{\bar{E}_{Si}}{\bar{E}_s} + b\frac{\bar{E}_{Si}}{\bar{E}_s}\frac{h}{H}}. \tag{6}$$

where a and b are fitting parameters. Fitting FEM results yields $a = 5.46 \times 10^{-5}$ and $b = 0.428$, which makes Eq. (6) a universal

expression to capture both $\varepsilon_{avg}/\varepsilon_{app}$ and $\varepsilon_{max}/\varepsilon_{app}$ (Fig. 2D), over wide ranges of $\bar{E}_{Si}/\bar{E}_s$ and h/H, provided $L \gg H$. Some important conclusions can be drawn from Fig. 2D: first, when the substrate stiffness is close to silicon, both $\varepsilon_{avg}/\varepsilon_{app}$ and $\varepsilon_{max}/\varepsilon_{app}$ approach 1; when the substrate becomes extremely soft or extremely thin, $\varepsilon/\varepsilon_{app}$ can be reduced by orders of magnitude, and will eventually die out.

With the two semi-analytical solutions given by Eqs. (5) and (6), it is useful to plot them as functions of L/h and compare them with FEM results as shown in Fig. 2E. It is clear that Eqs. (5) and (6) can successfully predict the FEM results, except the transition zone, i.e., mediocre L, which is consistent with the assumptions made to derive those two equations.

To discuss the tradeoff between GF and stretchability, we can relate GF to $\varepsilon_{avg}/\varepsilon_{app}$ as [82].

$$GF = GF_{Si}\frac{\varepsilon_{avg}}{\varepsilon_{app}}, \tag{7}$$

and relate stretchability (i.e., critical applied strain-to-rupture), ε_{app}^{cr}, to $\varepsilon_{max}/\varepsilon_{app}$ as [82]

$$\varepsilon_{app}^{cr} = \frac{\varepsilon_{cr}}{\varepsilon_{max}/\varepsilon_{app}}. \tag{8}$$

For the purpose of illustration, we have to assume some reasonable numbers for the intrinsic properties for silicon, including $GF_{Si} = 100$ [83] and critical strain-to-rupture $\varepsilon_{cr} = 1\%$. Fig. 2F plots the GF and ε_{app}^{cr} together as functions of E_s with everything else fixed. The tradeoff between the two is very clear: when the substrate is soft, the stretchability can be high but the GF is low and when the substrate is stiff, the stretchability is small but the GF can be enhanced. Choosing the right E_s, L, and H for stretchable strain gauges depends on the well anticipated performance metrics such as the system stiffness, stretchability, GF, as well as the fabrication preference such as the patterning resolution, and the thickness of silicon.

Although the stretchability and GF always go opposite directions, a concept of strain isolation has been introduced to break the limitation of low stretchability on stiff substrates [76,77]. Here we consider the stiff substrates to be materials like Kapton or PET, which have high modulus but are still stretchable up to tens of percent as long as large enough forces are applied. When a very soft later is placed in between the stiff islands and the stiff substrate, the tensile strain in the stiff substrate cannot be fully transferred to the stiff islands attributing to the enormous shear inside the soft interlayer. The effect of strain transfer reduction depends on the thickness and compliance of the interlayer, which has been successfully formulated [77].

The generic mechanics formulation given in this section is applicable to predict strains in any polymer-bonded stiff islands as long as linear elasticity and small deformation can be assumed. Delamination analysis are also available for single [94,95] or periodic [90,96] islands bonded to polymer substrates, which are not very recent results and hence will not be discussed in details here. More studies are needed to reveal the strain and delamination in polymer-bonded stiff islands when subjected to large deformation.

3. Stretchable serpentines

While patterning stiff membranes into isolated islands on soft substrates is an effective way for strain management, the functional components are discrete and hence lack of communication. The best way to build continuous, stretchable structure out of stiff materials is the serpentine design, i.e., patterning the blanket membranes into continuous but meandering ribbons [46,54]. When the polymer substrate is stretched, serpentine wires/ribbons can rotate in plane as well as buckle out of plane to accommodate the applied deformation, resulting in greatly reduced strains as well as much lower effective stiffness. In addition to serpentine-shaped, metal-based interconnects [46,54,67,97–100], electrophysiological or thermal sensing electrodes [58–61], or micro-heaters [101,102], silicon-based solar cells and amplifiers [58], zinc oxide-based nanogenerators [103], and graphene-based interconnects [104] can all be patterned into serpentine shapes using conventional photolithography and etching methods [46,58,104]. In addition to polymer-bonded serpentines, freestanding stretchable serpentine network can find applications in deployable sensor networks [75,105] and coronary stents [106]. In these two cases, the serpentine thickness is much larger than the width, and the large expandability mostly comes from the in-plane rigid body rotation of the serpentine arms. Serpentine structure now becomes the most effective mechanism to enhance the stretchability of any type of intrinsically stiff materials. In fact, serpentine structures offer more than just stretchability and compliance. Unlike flexible or bendable sheets only able to conform to cylindrical surfaces, a stretchable structure can also intimately and noninvasively conform to 3D curvilinear surfaces such as a human fist [75] or the fine wrinkles on the surface of a skin replica [61]. Although serpentines have been widely used as the stretchable configuration of stiff materials, the designs of the serpentine shape are still largely empirical. According to existing studies, the applied strain-to-rupture of metallic serpentine ribbons varies from 54% to 1600%, depending on the geometric parameters such as ribbon width, arc radius, and arm length substrate support [46,54,75,97,98,100]. The effects of serpentine shape and substrate constraint on serpentine stretchability and compliance have been studied by theoretical, numerical, and experimental means, as discussed in the follows.

3.1. Freestanding serpentines

Our discussion will begin with a fundamental mechanics study of freestanding, thick serpentine ribbons whose strain and compliance can be analytically obtained through curved beam (CB) theory, as shown in Fig. 3 [107]. Fig. 3A depicts a unit cell cut out of a one-directional periodic serpentine ribbon whose geometry can be completely defined by four parameters: the ribbon width w, the arc radius R, the arc angle α, and the arm length l. The end-to to-end distance of a unit cell is denoted by S. When this unit cell is subjected to a tensile displacement u_0 at each end, the effective applied strain ε_{app} is defined as

$$\varepsilon_{app} = \frac{2u_0}{S}. \tag{9}$$

Therefore a straight ribbon (i.e. $\alpha = -90°$) of length S should have a uniform strain of ε_{app} if the end effects are neglected. Taking advantage of symmetry, a unit cell can ultimately be represented by a quarter cell with fixed boundary at the axis of symmetry and a displacement of $u_0/2$ at the end, as shown in Fig. 3B. The reaction force is named P in Fig. 3B. Assuming linear elastic material and small deformation, through CB theory, the normalized stiffness and maximum strain in the serpentine can be obtained analytically as [107]:

$$\frac{P}{P'} = \frac{\frac{w}{R}\left(\cos\alpha - \frac{l}{2R}\sin\alpha\right)}{2\left[\begin{array}{l}\cos^2\alpha\left(\frac{l^3}{2R^3} + 3\left(\frac{\pi}{2}+\alpha\right)\frac{l^2}{R^2} + 12\frac{l}{R} - 12\left(\frac{\pi}{2}+\alpha\right)\right) \\ +\sin 2\alpha\left(6\left(\frac{\pi}{2}+\alpha\right)\frac{l}{R}+9\right) \\ +\frac{w^2}{R}\left[\left(\frac{\pi}{2}+\alpha\right)\left(\frac{l}{2R}\cos\alpha+\sin\alpha\right)^2 + \frac{l}{2R}\left(\sin\alpha + \frac{3\bar{E}}{2G}\cos\alpha\right)\right] + 18\left(\frac{\pi}{2}+\alpha\right)\end{array}\right]}, \tag{10}$$

where $P' = 2\bar{E}wu_0/S$ represents the reaction force needed for the linear counterpart of the serpentine to elongate by $2u_0$, and

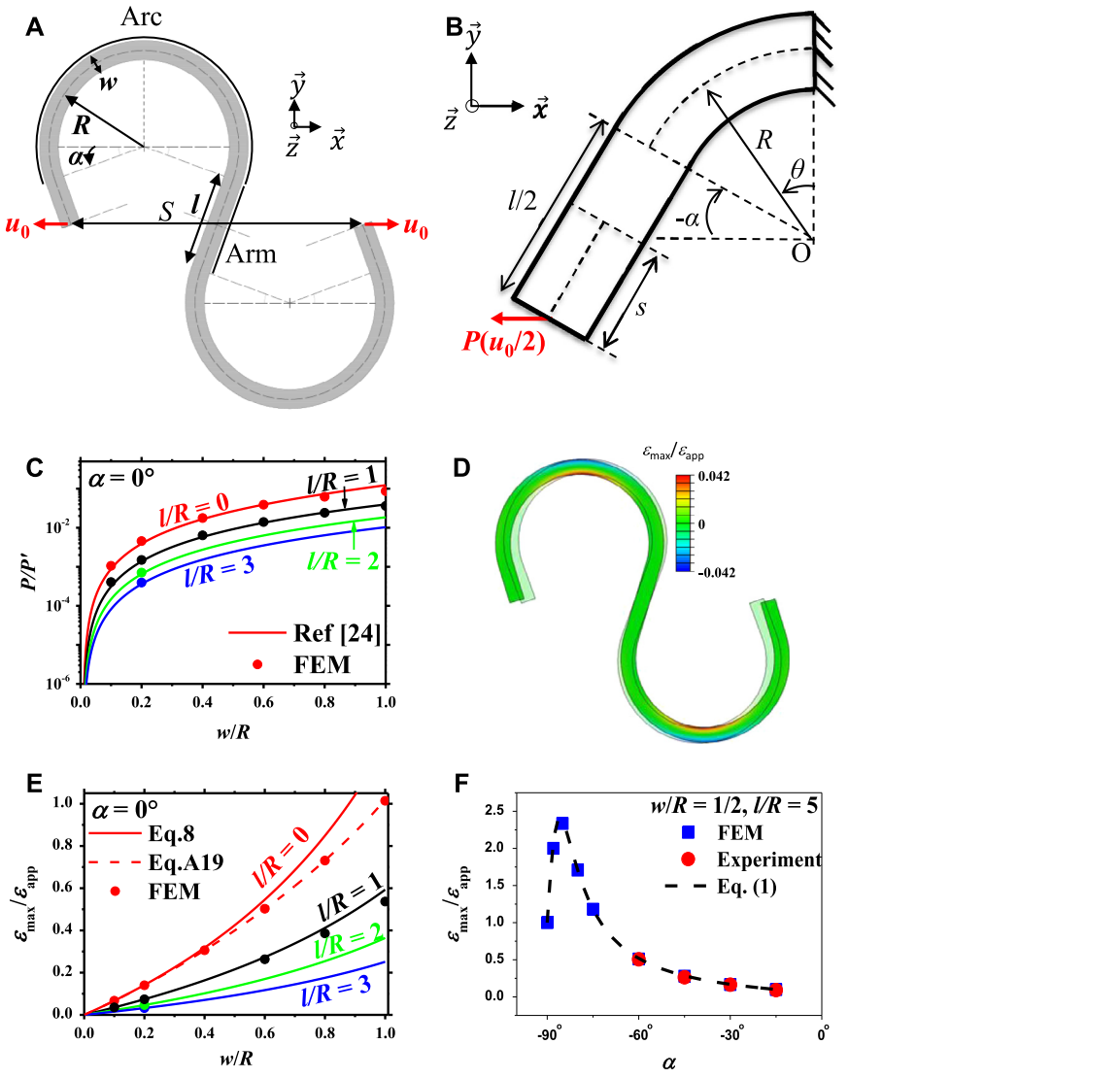

Fig. 3. 2D plane strain model of freestanding, thick serpentines [107]. (A) Geometric parameters and boundary conditions of a unit cell. (B) Simplified model due to symmetry and antisymmetry. (C) FEM and analytical results indicate that normalized serpentine stiffness can be tuned over orders of magnitude. (D) FEM strain distribution in a representative serpentine with maximum strain at the inner crest of the arc. (E) FEM and analytical results suggest normalized maximum strain is monotonic with w/R and l/R. (F) Experimental, FEM, and analytical results illustrate that the normalized maximums strain can be non-monotonic with respect to the arc angle α, and serpentine sometimes can be less stretchable than their straight counterparts.

$$\frac{\varepsilon_{\max}}{\varepsilon_{\text{app}}}=\frac{\frac{w}{R}\left[\frac{12}{2-\frac{w}{R}}+\left(\frac{12}{2-\frac{w}{R}}-\frac{w}{R}\right)\left(\sin\alpha+\frac{l}{2R}\cos\alpha\right)\right]\left(\cos\alpha-\frac{l}{2R}\sin\alpha\right)}{\left[\begin{array}{l}\cos^2\alpha\left(\frac{l^3}{2R^3}+3\left(\frac{\pi}{2}+\alpha\right)\frac{l^2}{R^2}+12\frac{l}{R}-12\left(\frac{\pi}{2}+\alpha\right)\right)\\+\sin 2\alpha\left(6\left(\frac{\pi}{2}+\alpha\right)\frac{l}{R}+9\right)\\+\frac{w^2}{R}\left[\left(\frac{\pi}{2}+\alpha\right)\left(\frac{l}{2R}\cos\alpha+\sin\alpha\right)^2+\frac{l}{2R}\left(\sin\alpha+\frac{3\bar{E}}{2G}\cos\alpha\right)\right]+18\left(\frac{\pi}{2}+\alpha\right)\end{array}\right]}. \tag{11}$$

Such closed form analytical results have found excellent agreement with FEM and experimental results as shown in Fig. 3C–F. It is evident in Fig. 3C that freestanding serpentines with smaller width and longer arms (compared to the arc radius) are more compliant. More impressively, Fig. 3C indicates that the effective stiffness can be reduced by orders of magnitude by simply changing a straight ribbon into serpentine shapes – this is why metal or silicon based serpentines can be made as soft as skins [58] and tissues [65]. The strain distribution in a representative serpentine unit cell obtained by FEM is given by Fig. 3D. It is obvious that the maximum strain in a freestanding, plane strain serpentine always occurs at the inner crest of the arc, which is exactly where 3D printed serpentine ribbons break when experimentally pulled. Fig. 3E suggests that the FEM results of the maximum strain match perfectly with the elasticity theory but not with the CB theory when the ratio w/R is bigger than 1/2. Fortunately, all of the commonly used serpentine shapes in stretchable sensors are well within $w/R < 1/2$, so that the CB theory can accurately capture the maximum strain in these serpentines. Although narrower and longer-armed serpentines also exhibit smaller strains, the strain reduction by serpentine is not as significant as the stiffness reduction when Fig. 3C and E are compared. The effect of the arc angle α is illustrated by Fig. 3F. The experimental results are obtained by recording the applied strain-to-rupture of 3D printed thick serpentine ribbons under uniaxial tension. Two observations can be readily made: first, while the effects of w/R and l/R are monotonic, the effect of α is not always monotonic; second, when α is close to $-90°$, i.e., when the serpentine approaches a linear ribbon, the maximum strain in the serpentine may exceed the applied strain, meaning the serpentine is less stretchable compared to their

straight counterpart. As a result, it is important for us to realize that not all serpentines can help reduce strains and the design of the serpentine needs to be rationalized.

Fig. 4 gives two distinctive serpentine designs [107]. Limited by the fabrication resolution and conductance requirement, serpentines cannot be made infinitely narrow. Therefore if there is no other limitations, the most effective way to build utmost stretchable serpentine is to use extremely long arms, as shown in Fig. 4A. The maximum strain as a function of the arm length is given by Fig. 4B, which shows that it is possible to achieve orders of magnitude enhancement in stretchability if the arm length can be made ten- or hundred-fold of the arc radius. This finding explains why the serpentines in the spider-web-like SHM sensor network can be stretched up to 1600% without losing electrical conductivity, as shown in Fig. 1D [75]. In many other circuit layout, however, there will be real estate limitations. In these cases, Fig. 4C and D offers an optimization strategy. To solve for the three unknowns, α, w/R, and l/R, three equations can be established to formulate the optimization problem: (i) the distance between the two nearest ribbons, $X \geqslant 0$; (ii) the breadth of the serpentine is limited, e.g., $Y/w = 10$; (iii) minimization of $\varepsilon_{max}/\varepsilon_{app}$, i.e. minimizing the values given by Eq. (11). Solving the three equations simultaneously yields the optimized shape given by Fig. 4D. Shape optimization under other constraints can be formulated following similar procedures.

When serpentine ribbons are very thin compared to their width, as in most bio-integrated sensors, freestanding serpentines will buckle out of plane to avoid high-strain-energy in-plane bending by developing low-strain-energy out-of-plane bending and twisting. Buckling and postbuckling theories and FEM have been developed to address this problem [55,108,109]. To enhance the areal coverage of functional serpentines without compromising the multidirectional stretchability, a concept of self-similar or fractal serpentines have been proposed, which has also greatly enhanced the topologies of serpentine designs [100,110–112]. So far, the optimization theories for freestanding, interlaced serpentine networks are still lacking.

3.2. Polymer-bonded serpentines

The mechanical behaviors of polymer-bonded serpentines are expected to be very different from the freestanding ones. The mechanics study of polymer-bonded or polymer-embedded serpentines dated back to 2004 [54]. Since then, a few experiments and FEM have been conducted to provide insights into the shape-dependent mechanical behaviors of polymer-supported metal-based serpentines [46,75,97–99,113–115]. Other than metallic serpentines, ceramic serpentines start to gain popularity as stretchable solar cells [58], amplifiers [58], and nanogenerators [103]. But so far there is little experimental mechanics investigation to reveal the stretchability of polymer-bonded brittle serpentine thin films due to the difficulty to fabricate and handle brittle serpentine thin films on soft polymer substrates. We have used indium tin oxide (ITO) as a model brittle material to study the mechanics of polymer-bonded brittle serpentines [116].

Thin ITO films have been a popular electrode material in flat panel displays [117] and solar cells [118] attributing to their combined high electrical conductivity and optical transparency. However, ITO is not mechanically favorable in flexible/stretchable electronics due to its brittle nature. Cracks were observed at applied tensile strains around 1% in polymer-supported blanket thin ITO films [106,119]. Resistance vs. applied strain curves have been widely adopted to indicate the stretchability of conductive thin films such as metal [48,49,120] and ITO [106]. Our experimental procedures are summarized in Fig. 5A–D [116]. After taking the ITO coated PI substrate (Kapton) out of the sputter chamber, the

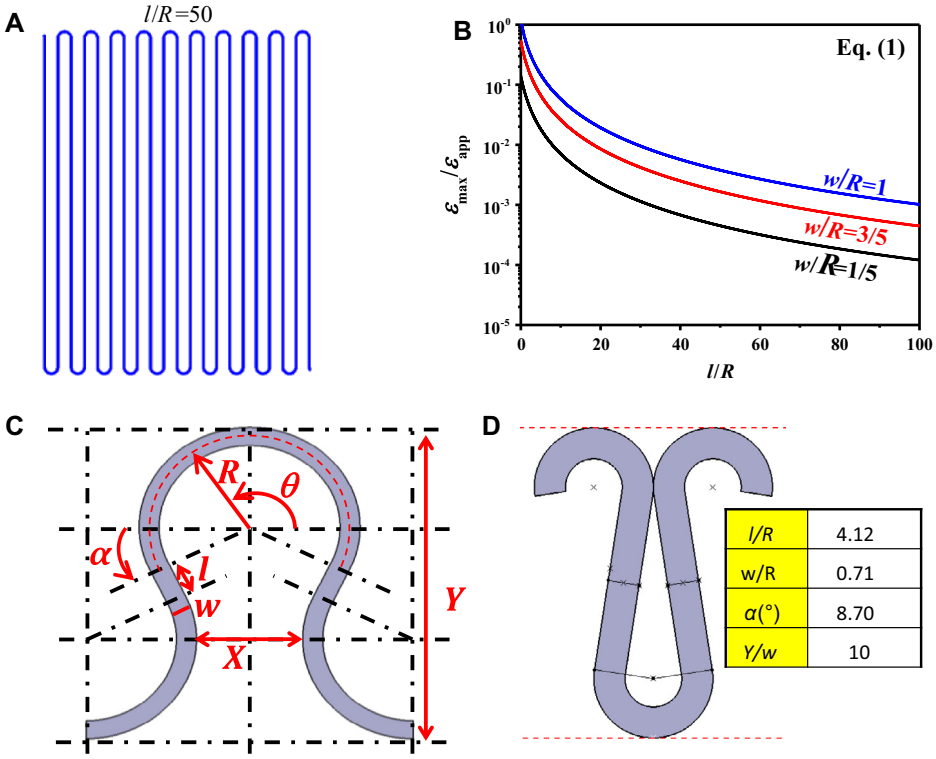

Fig. 4. Optimization of freestanding, thick serpentines [107]. (A) A representative freestanding long-armed serpentine. (B) The strain in such serpentines can be dropped by orders of magnitude. (C) Geometric drawing to illustrate the gap between the nearest ribbon, X, and the breadth of the serpentine, Y. (D) Analytically optimized serpentine shape under X and Y constraints and strain minimization.

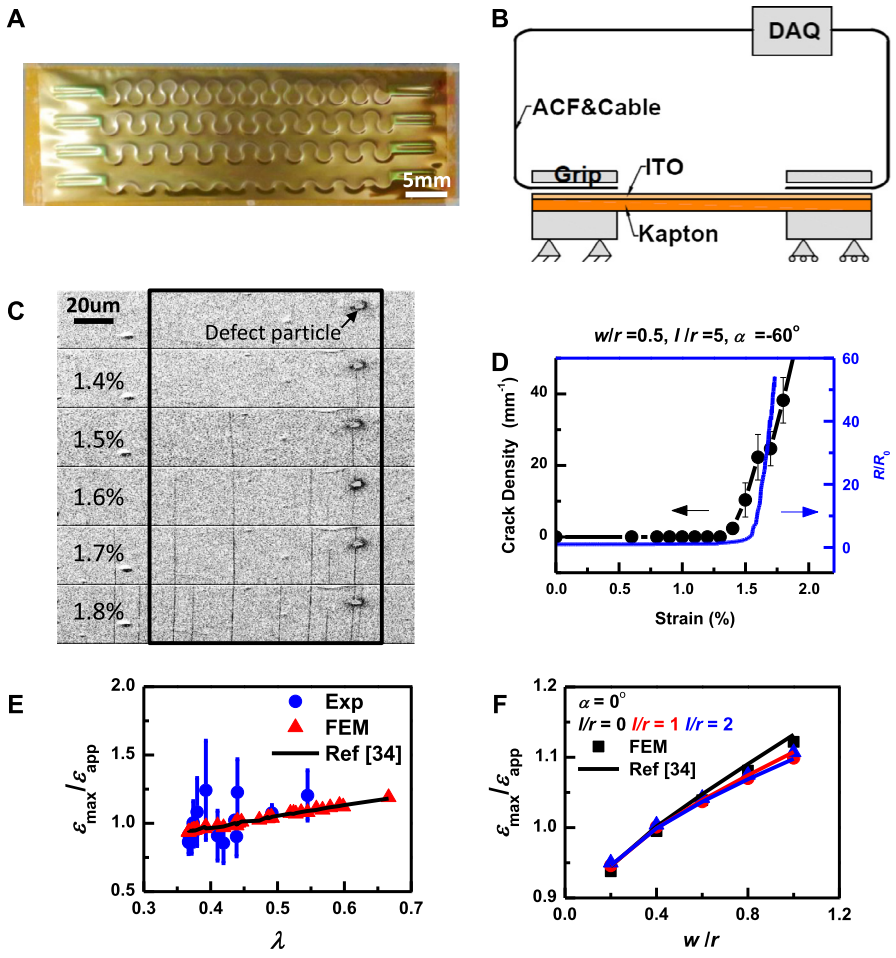

Fig. 5. Experimental mechanics of brittle serpentines on stiff substrate [116]. (A) Top view of a group of four ITO serpentine thin films sputtered on a Kapton substrate. (B) Schematics of the experimental setup for the *in situ* electrical resistance measurement of the ITO serpentines subjected to uniaxial tension test. (C) A sequence of SEM snapshots showing the evolution of crack density with increased applied strain. (D) curves of crack density/resistance vs. applied strain where the critical applied strain-to-rupture (i.e., stretchability) is determined as the strain at which the two curves blow up. (E) Comparing the empirical strain-geometry relation with experimental and FEM results. (F) While the effect of w/r is small and monotonic, the effect of l/r is almost negligible for serpentines bonded to stiff substrates.

straight specimens are cut into long rectangular strips and the serpentine specimens are cut into rectangular pieces each including a group of four or five serpentine ribbons with systematically varied shapes, as shown in Fig. 5A. A schematic of the tension test with *in situ* electrical resistance measurement is shown in Fig. 5B. According to a sequence of scanning electron microscope (SEM) images (Fig. 5C), the correlation between crack density and electrical resistance can be found in Fig. 5D. Despite of the small lag, the resistance is able to capture the failure of the ITO serpentine in a much more experimentally economic way compared to the crack density method.

Using FEM to model a unit cell of the Kapton-supported ITO serpentine subjected to a uniaxial tensile strain, ε_{app}, reveals that the strain concentration always occurs at the inner crest of the arc, which is consistent with our experimental observation of preferred crack initiation sites. Similar conclusion has also been drawn for freestanding serpentines as discussed in Section 3.1 [107]. A series of FEMs are performed for systematically varied serpentine shapes. An empirical equation is fitted based on the FEM results as discussed in [116]. The comparison between experiments, FEM, and the empirical equation is given by Fig. 5E. All of the FEM results are able to fall on the linear curve represented by the empirical equation. The experimental data also demonstrates reasonable agreement with limited scatter. This plot is a direct validation of our empirical relation between strain and geometry. Due to the constraint from the stiff Kapton substrate, the arm rotation is completely suppressed and hence the geometric effect on serpentine stretchability is minimum compared with freestanding ones. Fig. 5F plots $\varepsilon_{max}/\varepsilon_{app}$ as a function of w/r with different l/r using both the FEM results and the empirical equation. It is evident that w/r always has a monotonic effect on $\varepsilon_{max}/\varepsilon_{app}$ – smaller strains in narrow ribbons. Another important finding is that when w/r is beyond about 0.4, $\varepsilon_{max}/\varepsilon_{app}$ will be beyond 1, which means the stretchability of the serpentine will actually be lower than their straight counterpart, indicating a strain augmentation instead of strain reduction effect. Compared with the effect of w/r, the effects of arm length l/r and α (not shown) are not as significant, especially when w/r is small. Some non-monotonic effect of α have been uncovered by FEM, which has also been successfully captured by our empirical equation (not shown). The key message from this study is that stiff serpentines directly bonded to stiff substrates like Kapton or PET are in general not more stretchable than their linear counterpart and many cases could be even worse. Serpentines will be stretchable when integrated on a very soft substrate or when they are allowed to detach from a stiff substrate.

4. Conclusion

This review article tries to address the mechanics of the most popular structural design of stretchable sensors: the island plus

serpentine design. We have discussed the mechanics of polymer-supported islands, freestanding serpentines, and polymer-supported brittle serpentines, respectively. The small strain analysis provided in this paper are generic to all types of stiff thin films including ceramic, metallic, and even two-dimensional nanomembranes as long as continuum mechanics applies. In general, we find softer substrates and smaller features can yield lower strains and hence larger stretchability. We have also touched the tradeoff between mechanics and functionality and we recognize that the simultaneous optimization of structure and performance still remains a grand challenge in this field, which can only be addressed through multidisciplinary research.

Acknowledgements

N.L. acknowledges the support from US NSF CMMI #1351875, the US NSF NASCENT Center (EEC #1160494), and the 3M Non-Tenured Faculty Award.

References

[1] Garnier F, Hajlaoui R, Yassar A, Srivastava P. All-polymer field-effect transistor realized by printing techniques. Science 1994;265(5179):1684–6. http://dx.doi.org/10.1126/science.265.5179.1684. PubMed PMID: WOS:A1994PG28400022.

[2] Bao ZN, Feng Y, Dodabalapur A, Raju VR, Lovinger AJ. High-performance plastic transistors fabricated by printing techniques. Chem Mater 1997;9(6):1299–301. http://dx.doi.org/10.1021/Cm9701163. PubMed PMID: WOS:A1997XE92200003.

[3] Reuss RH, Chalamala BR, Moussessian A, Kane MG, Kumar A, Zhang DC, et al. Macroelectronics: perspectives on technology and applications. Proc IEEE 2005;93(7):1239–56. http://dx.doi.org/10.1109/Jproc.2005.851237. PubMed PMID: WOS:000230466300002.

[4] Rogers JA, Bao Z, Baldwin K, Dodabalapur A, Crone B, Raju VR, et al. Paper-like electronic displays: large-area rubber-stamped plastic sheets of electronics and microencapsulated electrophoretic inks. P Natl Acad Sci USA 2001;98(9):4835–40. http://dx.doi.org/10.1073/pnas.091588098. PubMed PMID: WOS:000168311500008.

[5] Gelinck GH, Huitema HEA, Van Veenendaal E, Cantatore E, Schrijnemakers L, Van der Putten JBPH, et al. Flexible active-matrix displays and shift registers based on solution-processed organic transistors. Nat Mater 2004;3(2):106–10. http://dx.doi.org/10.1038/Nmat1061. PubMed PMID: WOS:000188668200018.

[6] Dimitrakopoulos CD, Malenfant PRL. Organic thin film transistors for large area electronics. Adv Mater 2002;14(2):99–117. http://dx.doi.org/10.1002/1521-4095(20020116)14:2<99::Aid-Adma99>3.0.Co;2-9. PubMed PMID: WOS:000173687600007.

[7] Forrest SR. The path to ubiquitous and low-cost organic electronic appliances on plastic. Nature 2004;428(6986):911–8. http://dx.doi.org/10.1038/Nature02498. PubMed PMID: WOS:000221083000032.

[8] Service RF. Materials science – inorganic electronics begin to flex their muscle. Science 2006;312(5780):1593–4. http://dx.doi.org/10.1126/science.312.5780.1593. PubMed PMID: WOS:000238288600012.

[9] Sun YG, Rogers JA. Inorganic semiconductors for flexible electronics. Adv Mater 2007;19(15):1897–916. http://dx.doi.org/10.1002/adma.200602223. PubMed PMID: WOS:000248706900001.

[10] Kim DH, Ahn JH, Choi WM, Kim HS, Kim TH, Song JZ, et al. Stretchable and foldable silicon integrated circuits. Science 2008;320(5875):507–11. http://dx.doi.org/10.1126/science.1154367. PubMed PMID: WOS:000255249300044.

[11] Viventi J, Kim DH, Vigeland L, Frechette ES, Blanco JA, Kim YS, et al. Flexible, foldable, actively multiplexed, high-density electrode array for mapping brain activity *in vivo*. Nat Neurosci 2011;14(12):1599–605. http://dx.doi.org/10.1038/Nn.2973. PubMed PMID: WOS:000297546300021.

[12] Yoon J, Baca AJ, Park SI, Elvikis P, Geddes JB, Li LF, et al. Ultrathin silicon solar microcells for semitransparent, mechanically flexible and microconcentrator module designs. Nat Mater 2008;7(11):907–15. http://dx.doi.org/10.1038/Nmat2287. PubMed PMID: WOS:000260472800025.

[13] Park SI, Xiong YJ, Kim RH, Elvikis P, Meitl M, Kim DH, et al. Printed assemblies of inorganic light-emitting diodes for deformable and semitransparent displays. Science 2009;325(5943):977–81. http://dx.doi.org/10.1126/science.1175690. PubMed PMID: WOS:000269242800041.

[14] Koo M, Park KI, Lee SH, Suh M, Jeon DY, Choi JW, et al. Bendable inorganic thin-film battery for fully flexible electronic systems. Nano Lett 2012;12(9):4810–6. http://dx.doi.org/10.1021/Nl302254v. PubMed PMID: WOS:000308576000065.

[15] Dagdeviren C, Yang BD, Su YW, Tran PL, Joe P, Anderson E, et al. Conformal piezoelectric energy harvesting and storage from motions of the heart, lung, and diaphragm. P Natl Acad Sci USA 2014;111(5):1927–32. http://dx.doi.org/10.1073/pnas.1317233111. PubMed PMID: WOS:000330587600066.

[16] Timoshenko S. History of strength of materials. New York: McGraw-Hill; 1953.

[17] Li L, Lin H, Qiao S, Zou Y, Danto S, Richardson K, et al. 3-D integrated flexible glass photonics. Nat Photonics 2014.

[18] Khang DY, Jiang HQ, Huang Y, Rogers JA. A stretchable form of single-crystal silicon for high-performance electronics on rubber substrates. Science 2006;311(5758):208–12. http://dx.doi.org/10.1126/science.1121401. PubMed PMID: WOS:000234722200036.

[19] Sun YG, Choi WM, Jiang HQ, Huang YGY, Rogers JA. Controlled buckling of semiconductor nanoribbons for stretchable electronics. Nat Nanotechnol 2006;1(3):201–7. http://dx.doi.org/10.1038/nnano.2006.131. PubMed PMID: WOS:000243902800016.

[20] Sun Y, Kumar V, Adesida I, Rogers J. Buckled and wavy ribbons of GaAs for high-performance electronics on elastomeric substrates. Adv Mater 2006;18(21). http://dx.doi.org/10.1002/adma.20060064. 2857-+. PubMed PMID: WOS:000242292800012.

[21] Choi W, Song J, Khang D, Jiang H, Huang Y, Rogers J. Biaxially stretchable "Wavy" silicon nanomembranes. Nano Lett 2007;7(6):1655–63. http://dx.doi.org/10.1021/nl0706244. PubMed PMID: WOS:000247186800040.

[22] Watanabe M, Shirai H, Hirai T. Wrinkled polypyrrole electrode for electroactive polymer actuators. J Appl Phys 2002;92(8):4631–7. http://dx.doi.org/10.1063/1.1505674. PubMed PMID: WOS:000178318000067.

[23] Lacour SP, Jones J, Suo Z, Wagner S. Design and performance of thin metal film interconnects for skin-like electronic circuits. Ieee Electr Device L 2004;25(4):179–81. http://dx.doi.org/10.1109/Led.2004.825190. PubMed PMID: WOS:000220478000007.

[24] Lacour SP, Jones J, Wagner S, Li T, Suo ZG. Stretchable interconnects for elastic electronic surfaces. Proc IEEE 2005;93(8):1459–67. PubMed PMID: WOS:000230737600011.

[25] Lacour SP, Wagner S, Huang ZY, Suo Z. Stretchable gold conductors on elastomeric substrates. Appl Phys Lett 2003;82(15):2404–6. http://dx.doi.org/10.1063/1.1565683. PubMed PMID: WOS:000182104900012.

[26] Bowden N, Brittain S, Evans AG, Hutchinson JW, Whitesides GM. Spontaneous formation of ordered structures in thin films of metals supported on an elastomeric polymer. Nature 1998;393(6681):146–9. PubMed PMID: WOS:000073619900041.

[27] Bowden N, Huck WTS, Paul KE, Whitesides GM. The controlled formation of ordered, sinusoidal structures by plasma oxidation of an elastomeric polymer. Appl Phys Lett 1999;75(17):2557–9. http://dx.doi.org/10.1063/1.125076. PubMed PMID: WOS:000083185900013.

[28] Huck WTS, Bowden N, Onck P, Pardoen T, Hutchinson JW, Whitesides GM. Ordering of spontaneously formed buckles on planar surfaces. Langmuir 2000;16(7):3497–501. http://dx.doi.org/10.1021/la991302l. PubMed PMID: WOS:000086225200076.

[29] Allen HG. Analysis and design of structural sandwich panels. New York: Pergamon; 1969.

[30] Hutchinson JW, Suo Z. Mixed-mode cracking in layered materials. Adv Appl Mech 1992;29:63–191. PubMed PMID: WOS:A1992BZ96U00002.

[31] Gioia G, Ortiz M. Delamination of compressed thin films. Adv Appl Mech 1997;33:119–92. http://dx.doi.org/10.1016/S0065-2156(08)70386-7. PubMed PMID: WOS:A1997BH79H00003.

[32] Audoly B. Mode-dependent toughness and the delamination of compressed thin films. J Mech Phys Solids 2000;48(11):2315–32. http://dx.doi.org/10.1016/S0022-5096(00)00007-7. PubMed PMID: WOS:000089246300005.

[33] Ohzono T, Shimomura M. Ordering of microwrinkle patterns by compressive strain. Phys Rev B 2004;69(13). doi: Artn 132202. PubMed PMID: WOS:000221278100004, 10.1103/Physrevb.69.13220.

[34] Huang R. Kinetic wrinkling of an elastic film on a viscoelastic substrate. J Mech Phys Solids 2005;53(1):63–89. http://dx.doi.org/10.1016/j.jmps.2004.06.007. PubMed PMID: WOS:000226034500004.

[35] Huang ZY, Hong W, Suo Z. Nonlinear analyses of wrinkles in a film bonded to a compliant substrate. J Mech Phys Solids 2005;53(9):2101–18. http://dx.doi.org/10.1016/j.jmps.2005.03.007. PubMed PMID: WOS:000230939400007.

[36] Jiang H, Khang D, Song J, Sun Y, Huang Y, Rogers J. Finite deformation mechanics in buckled thin films on compliant supports. P Natl Acad Sci USA 2007;104(40):15607–12. http://dx.doi.org/10.1073/pnas.0702927104. PubMed PMID: WOS:000249942700005.

[37] Song J, Jiang H, Choi WM, Khang DY, Huang Y, Rogers JA. An analytical study of two-dimensional buckling of thin films on compliant substrates. J Appl Phys 2008;103(1). http://dx.doi.org/10.1063/1.282805. doi: Artn 014303. PubMed PMID: WOS:000252890700079.

[38] Song J, Jiang H, Liu Z, Khang D, Huang Y, Rogers J, et al. Buckling of a stiff thin film on a compliant substrate in large deformation. Int J Solids Struct 2008;45(10):3107–21. http://dx.doi.org/10.1016/j.ijsolstr.2008.01.023. PubMed PMID: WOS:000255323900020.

[39] Xiao J, Carlson A, Liu ZJ, Huang Y, Jiang H, Rogers JA. Stretchable and compressible thin films of stiff materials on compliant wavy substrates. Appl Phys Lett 2008;93(1). http://dx.doi.org/10.1063/1.295582. doi: Artn 013109. PubMed PMID: WOS:000258184600051.

[40] Mei HX, Landis CM, Huang R. Concomitant wrinkling and buckle-delamination of elastic thin films on compliant substrates. Mech Mater 2011;43(11):627–42. http://dx.doi.org/10.1016/j.mechmat.2011.08.003. PubMed PMID: WOS:000297000900001.

[41] Cao YP, Hutchinson JW. Wrinkling phenomena in neo-Hookean film/substrate bilayers. J Appl Mech-T Asme 2012;79(3). http://dx.doi.org/

10.1115/1.400596. doi: Artn 031019. PubMed PMID: WOS:000303261700020.
[42] Sun JY, Xia SM, Moon MW, Oh KH, Kim KS. Folding wrinkles of a thin stiff layer on a soft substrate. Proc Royal Soc –Math Phys Eng Sci 2012;468(2140):932–53. http://dx.doi.org/10.1098/rspa.2011.0567. PubMed PMID: WOS:000300820800002.
[43] Zang JF, Zhao XH, Cao YP, Hutchinson JW. Localized ridge wrinkling of stiff films on compliant substrates. J Mech Phys Solids 2012;60(7):1265–79. http://dx.doi.org/10.1016/j.jmps.2012.03.009. PubMed PMID: WOS:000304687700003.
[44] Cheng HY, Zhang YH, Hwang KC, Rogers JA, Huang YG. Buckling of a stiff thin film on a pre-strained bi-layer substrate. Int J Solids Struct 2014;51(18):3113–8. http://dx.doi.org/10.1016/j.ijsolstr.2014.05.012. PubMed PMID: WOS:000340141100010.
[45] Wang QM, Zhao XH. Phase diagrams of instabilities in compressed film-substrate systems. J Appl Mech-T Asme 2014;81(5). http://dx.doi.org/10.1115/1.402582. doi: Artn 051004. PubMed PMID: WOS:000333847000004.
[46] Kim DH, Song JZ, Choi WM, Kim HS, Kim RH, Liu ZJ, et al. Materials and noncoplanar mesh designs for integrated circuits with linear elastic responses to extreme mechanical deformations. P Natl Acad Sci USA 2008;105(48):18675–80. http://dx.doi.org/10.1073/pnas.0807476105. PubMed PMID: WOS:000261489100014.
[47] Li T, Suo Z. Ductility of thin metal films on polymer substrates modulated by interfacial adhesion. Int J Solids Struct 2007;44(6):1696–705. http://dx.doi.org/10.1016/j.ijsolstr.2006.07.022. PubMed PMID: WOS:000244576400002.
[48] Lu NS, Wang X, Suo Z, Vlassak J. Metal films on polymer substrates stretched beyond 50%. Appl Phys Lett 2007;91(22):221909. http://dx.doi.org/10.1063/1.2817234. Artn 221909 PubMed PMID: WOS:000251324600031.
[49] Lu NS, Suo ZG, Vlassak JJ. The effect of film thickness on the failure strain of polymer-supported metal films. Acta Mater 2010;58(5):1679–87. http://dx.doi.org/10.1016/j.actamat.2009.11.010. PubMed PMID: WOS:000274931200020.
[50] Lacour SP, Chan D, Wagner S, Li T, Suo ZG. Mechanisms of reversible stretchability of thin metal films on elastomeric substrates. Appl Phys Lett 2006;88(20). http://dx.doi.org/10.1063/1.220187. doi: Artn 204103. PubMed PMID: WOS:000237682100102.
[51] Ko HC, Stoykovich MP, Song JZ, Malyarchuk V, Choi WM, Yu CJ, et al. A hemispherical electronic eye camera based on compressible silicon optoelectronics. Nature 2008;454(7205):748–53. http://dx.doi.org/10.1038/Nature07113. PubMed PMID: WOS:000258228000041.
[52] Jung IW, Xiao JL, Malyarchuk V, Lu CF, Li M, Liu ZJ, et al. Dynamically tunable hemispherical electronic eye camera system with adjustable zoom capability. P Natl Acad Sci USA 2011;108(5):1788–93. http://dx.doi.org/10.1073/pnas.1015440108. PubMed PMID: WOS:000286804700011.
[53] Song YM, Xie YZ, Malyarchuk V, Xiao JL, Jung I, Choi KJ, et al. Digital cameras with designs inspired by the arthropod eye. Nature 2013;497(7447):95–9. http://dx.doi.org/10.1038/Nature12083. PubMed PMID: WOS:000318221500040.
[54] Gray DS, Tien J, Chen CS. High-conductivity elastomeric electronics. Adv Mater 2004;16(5):393. http://dx.doi.org/10.1002/adma.200306107. PubMed PMID: WOS:000220322900003.
[55] Li T, Suo ZG, Lacour SP, Wagner S. Compliant thin film patterns of stiff materials as platforms for stretchable electronics. J Mater Res 2005;20(12):3274–7. http://dx.doi.org/10.1557/Jmr.2005.0422. PubMed PMID: WOS:000233628600014.
[56] Rogers JA, Someya T, Huang YG. Materials and mechanics for stretchable electronics. Science 2010;327(5973):1603–7. http://dx.doi.org/10.1126/science.1182383. PubMed PMID: WOS:000275970600032.
[57] Suo ZG. Mechanics of stretchable electronics and soft machines. Mrs Bull 2012;37(3):218–25. http://dx.doi.org/10.1557/Mrs.2012.32. PubMed PMID: WOS:000302471900014.
[58] Kim DH, Lu NS, Ma R, Kim YS, Kim RH, Wang SD, et al. Epidermal electronics. Science 2011;333(6044):838–43. http://dx.doi.org/10.1126/science.1206157. PubMed PMID: WOS:000293785400031.
[59] Jeong JW, Yeo WH, Akhtar A, Norton JJS, Kwack YJ, Li S, et al. Materials and optimized designs for human-machine interfaces via epidermal electronics. Adv Mater 2013;25(47):6839–46. http://dx.doi.org/10.1002/adma.201301921. PubMed PMID: WOS:000328424600005.
[60] Webb RC, Bonifas AP, Behnaz A, Zhang YH, Yu KJ, Cheng HY, et al. Ultrathin conformal devices for precise and continuous thermal characterization of human skin. Nat Mater 2013;12(10):938–44. http://dx.doi.org/10.1038/Nmat3755. PubMed PMID: WOS:000324736000021.
[61] Yeo W-H, Kim Y-S, Lee J, Ameen A, Shi L, Li M, et al. Multi-functional electronics: multifunctional epidermal electronics printed directly onto the skin (adv. mater. 20/2013). Adv Mater 2013;25(20):2772. http://dx.doi.org/10.1002/adma.20137013.
[62] Son D, Lee J, Qiao S, Ghaffari R, Kim J, Lee JE, et al. Multifunctional wearable devices for diagnosis and therapy of movement disorders. Nat Nanotechnol 2014;9(5):397–404. http://dx.doi.org/10.1038/Nnano.2014.38. PubMed PMID: WOS:000336235800018.
[63] Xu S, Zhang YH, Jia L, Mathewson KE, Jang KI, Kim J, et al. Soft microfluidic assemblies of sensors, circuits, and radios for the skin. Science 2014;344(6179):70–4. http://dx.doi.org/10.1126/science.1250169. PubMed PMID: WOS:000333746100053.
[64] Ying M, Bonifas AP, Lu NS, Su YW, Li R, Cheng HY, et al. Silicon nanomembranes for fingertip electronics. Nanotechnology 2012;23(34):344004. http://dx.doi.org/10.1088/0957-4484/23/34/344004. Artn 344004 PubMed PMID: WOS:000307812000005.
[65] Kim DH, Ghaffari R, Lu NS, Wang SD, Lee SP, Keum H, et al. Electronic sensor and actuator webs for large-area complex geometry cardiac mapping and therapy. P Natl Acad Sci USA 2012;109(49):19910–5. http://dx.doi.org/10.1073/pnas.1205923109. PubMed PMID: WOS:000312347200019.
[66] Xu LZ, Gutbrod SR, Bonifas AP, Su YW, Sulkin MS, Lu NS, et al. 3D multifunctional integumentary membranes for spatiotemporal cardiac measurements and stimulation across the entire epicardium. Nat Commun 2014:5. http://dx.doi.org/10.1038/Ncomms432. doi: Artn 3329. PubMed PMID: WOS:000332668300022.
[67] Kim DH, Lu NS, Ghaffari R, Kim YS, Lee SP, Xu LZ, et al. Materials for multifunctional balloon catheters with capabilities in cardiac electrophysiological mapping and ablation therapy. Nat Mater 2011;10(4):316–23. http://dx.doi.org/10.1038/Nmat2971. PubMed PMID: WOS:000288744700023.
[68] Kim DH, Lu NS, Ghaffari R, Rogers JA. Inorganic semiconductor nanomaterials for flexible and stretchable bio-integrated electronics. Npg Asia Mater 2012;4:e15. http://dx.doi.org/10.1038/am.2012.27. PubMed PMID: WOS:000303612500004.
[69] Kim DH, Lu NS, Huang YG, Rogers JA. Materials for stretchable electronics in bioinspired and biointegrated devices. Mrs Bull 2012;37(3):226–35. http://dx.doi.org/10.1557/Mrs.2012.36. PubMed PMID: WOS:000302471900015.
[70] Kim DH, Ghaffari R, Lu NS, Rogers JA. Flexible and stretchable electronics for bio-integrated devices. Annu Rev Biomed Eng 2012;14:113–28.
[71] Lu N, Kim D-H. Flexible and stretchable electronics paving the way for soft robotics. Soft Robotics 2013;1(1):53–62. http://dx.doi.org/10.1089/soro.2013.0005.
[72] Lu N. Mechanics, materials, and functionalities of biointegrated electronics. Bridge Front Eng 2013;43:31.
[73] Kim J, Lee M, Rhim J, Wang P, Lu N, Kim D-H. Next-generation flexible neural and cardiac electrode arrays. Biomed Eng Lett 2014;4(2):95–108. http://dx.doi.org/10.1007/s13534-014-0132-4.
[74] Lanzara G, Feng J, Chang FK. Design of micro-scale highly expandable networks of polymer-based substrates for macro-scale applications. Smart Mater Struct 2010;19(4). http://dx.doi.org/10.1088/0964-1726/19/4/04501. doi: Artn 045013 PubMed PMID: WOS:000275842000013.
[75] Lanzara G, Salowitz N, Guo ZQ, Chang FK. A spider-web-like highly expandable sensor network for multifunctional materials. Adv Mater 2010;22(41):4643–8. http://dx.doi.org/10.1002/adma.201000661. PubMed PMID: WOS:000284002600014.
[76] Kim DH, Kim YS, Wu J, Liu ZJ, Song JZ, Kim HS, et al. Ultrathin silicon circuits with strain-isolation layers and mesh layouts for high-performance electronics on fabric, vinyl, leather, and paper. Adv Mater 2009;21(36):3703–9. http://dx.doi.org/10.1002/adma.200900405. PubMed PMID: WOS:000270441700015.
[77] Sun JY, Lu NS, Yoon J, Oh KH, Suo ZG, Vlassak JJ. Inorganic islands on a highly stretchable polyimide substrate. J Mater Res 2009;24(11):3338–42. http://dx.doi.org/10.1557/Jmr.2009.0417. PubMed PMID: WOS:000271352200011.
[78] Gleskova H, Wagner S, Suo Z. Failure resistance of amorphous silicon transistors under extreme in-plane strain. Appl Phys Lett 1999;75(19):3011–3. http://dx.doi.org/10.1063/1.125174. PubMed PMID: WOS:000083483900047.
[79] Bhattacharya R, Salomon A, Wagner S. Fabricating metal interconnects for circuits on a spherical dome. J Electrochem Soc 2006;153(3):G259–65.
[80] Hoyt JL, Nayfeh HM, Eguchi S, Aberg I, Xia G, Drake T, et al. Strained silicon MOSFET technology. International Electron Devices 2002 Meeting, Technical Digest. 2002:23–6. PubMed PMID: WOS:000185143400004.
[81] Jacobsen RS, Andersen KN, Borel PI, Fage-Pedersen J, Frandsen LH, Hansen O, et al. Strained silicon as a new electro-optic material. Nature 2006;441(7090):199–202. http://dx.doi.org/10.1038/Nature04706. PubMed PMID: WOS:000237418800041.
[82] Yang S, Lu N. Gauge factor and stretchability of silicon-on-polymer strain gauges. Sensors 2013;13:8577–94. http://dx.doi.org/10.3390/s130708577.
[83] Won SM, Kim HS, Lu NS, Kim DG, Del Solar C, Duenas T, et al. Piezoresistive strain sensors and multiplexed arrays using assemblies of single-crystalline silicon nanoribbons on plastic substrates. Ieee T Electron Dev 2011;58(11):4074–8. http://dx.doi.org/10.1109/Ted.2011.2164923. PubMed PMID: WOS:000296099400057.
[84] Window AL. Strain gauge technology. London, England: Elsevier Applied Science; 1992.
[85] Smith CS. Piezoresistance effect in germanium and silicon. Phys Rev 1954;94(1):42–9.
[86] Kanda Y. Piezoresistance effect of silicon. Sensor Actuat – Phys 1991;28(2):83–91. http://dx.doi.org/10.1016/0924-4247(91)85017-I. PubMed PMID: WOS:A1991GD46000002.
[87] Middelhoek S. Silicon Sensors. Delft, The Netherlands: Delft University; 1994.
[88] Yamada T, Hayamizu Y, Yamamoto Y, Yomogida Y, Izadi-Najafabadi A, Futaba DN, et al. A stretchable carbon nanotube strain sensor for human-motion detection. Nat Nanotechnol 2011;6(5):296–301. http://dx.doi.org/10.1038/Nnano.2011.36. PubMed PMID: WOS:000290301300010.
[89] Lu NS, Lu C, Yang SX, Rogers J. Highly sensitive skin-mountable strain gauges based entirely on elastomers. Adv Funct Mater 2012;22(19):4044–50. http://

dx.doi.org/10.1002/adfm.201200498. PubMed PMID: WOS:000309404000010.
[90] Lu NS, Yoon JI, Suo ZG. Delamination of stiff islands patterned on stretchable substrates. Int J Mater Res 2007;98(8):717–22. http://dx.doi.org/10.3139/146.101529. PubMed PMID: WOS:000249611600008.
[91] Yoon J, Zhang Z, Lu NS, Suo ZG. The effect of coating in increasing the critical size of islands on a compliant substrate. Appl Phys Lett 2007;90(21). http://dx.doi.org/10.1063/1.274291. doi: Artn 211912 PubMed PMID: WOS:000246775900029.
[92] Xia ZC, Hutchinson JW. Crack patterns in thin films. J Mech Phys Solids 2000;48(6–7):1107–31. http://dx.doi.org/10.1016/S0022-5096(99)00081-2. PubMed PMID: WOS:000086820000004.
[93] Handge UA. Analysis of a shear-lag model with nonlinear elastic stress transfer for sequential cracking of polymer coatings. J Mater Sci 2002;37(22):4775–82. http://dx.doi.org/10.1023/A:1020814314019. PubMed PMID: WOS:000178718800014.
[94] Yu HH, He MY, Hutchinson JW. Edge effects in thin film delamination. Acta Mater 2001;49(1):93–107. http://dx.doi.org/10.1016/S1359-6454(00)00293-7. PubMed PMID: WOS:000166681300010.
[95] Yu HH, Hutchinson JW. Delamination of thin film strips. Thin Solid Films 2003;423(1):54–63. http://dx.doi.org/10.1016/S0040-6090(02)00973-2. doi: Pii S0040-6090(02)00973-2 PubMed PMID: WOS:000182542300007.
[96] Sun JY, Lu NS, Yoon J, Oh KH, Suo ZG, Vlassak JJ. Debonding and fracture of ceramic islands on polymer substrates. J Appl Phys 2012;111(1). http://dx.doi.org/10.1063/1.367380. doi: Artn 013517. PubMed PMID: WOS:000299127200032.
[97] Brosteaux D, Axisa F, Gonzalez M, Vanfleteren J. Design and fabrication of elastic interconnections for stretchable electronic circuits. Ieee Electr Device L 2007;28(7):552–4. http://dx.doi.org/10.1109/Led.2007.897887. PubMed PMID: WOS:000247643900005.
[98] Hsu YY, Gonzalez M, Bossuyt F, Axisa F, Vanfleteren J, De Wolf I. *In situ* observations on deformation behavior and stretching-induced failure of fine pitch stretchable interconnect. J Mater Res 2009;24(12):3573–82. http://dx.doi.org/10.1557/Jmr.2009.0447. PubMed PMID: WOS:000272412500012.
[99] Hsu YY, Gonzalez M, Bossuyt F, Vanfleteren J, De Wolf I. Polyimide-enhanced stretchable interconnects: design, fabrication, and characterization. Ieee T Electron Dev 2011;58(8):2680–8. http://dx.doi.org/10.1109/Ted.2011.2147789. PubMed PMID: WOS:000293708500061.
[100] Xu S, Zhang YH, Cho J, Lee J, Huang X, Jia L, et al. Stretchable batteries with self-similar serpentine interconnects and integrated wireless recharging systems. Nat Commun 2013:4. doi: Artn 1543Doi 10.1038/Ncomms2553. PubMed PMID: WOS:000316616400111.
[101] Yu CJ, Duan Z, Yuan PX, Li YH, Su YW, Zhang X, et al. Electronically programmable, reversible shape change in two- and three-dimensional hydrogel structures. Adv Mater 2013;25(11):1541–6. http://dx.doi.org/10.1002/adma.201204180. PubMed PMID: WOS:000316215700002.
[102] Son D, Lee J, Qiao S, Ghaffari R, Kim J, Lee JE, et al. Multifunctional wearable devices for diagnosis and therapy of movement disorders. Nat Nanotechnol 2014;9:397–404.
[103] Ma T, Wang Y, Tang R, Yu H, Jiang H. Pre-patterned ZnO nanoribbons on soft substrates for stretchable energy harvesting applications. J Appl Phys 2013;113(20). doi: http://dx.doi.org/10.1063/1.4807320.
[104] Kim RH, Bae MH, Kim DG, Cheng HY, Kim BH, Kim DH, et al. Stretchable, transparent graphene interconnects for arrays of microscale inorganic light emitting diodes on rubber substrates. Nano Lett 2011;11(9):3881–6. http://dx.doi.org/10.1021/Nl202000u. PubMed PMID: WOS:000294790200064.
[105] Gonzalez M, Axisa F, Bossuyt F, Hsu YY, Vandevelde B, Vanfleteren J. Design and performance of metal conductors for stretchable electronic circuits. Circuit World 2009;35(1):22–9. http://dx.doi.org/10.1108/03056120910928699. PubMed PMID: WOS:000264252300004.
[106] Mani G, Feldman MD, Patel D, Agrawal CM. Coronary stents: a materials perspective. Biomaterials 2007;28(9):1689–710. http://dx.doi.org/10.1016/j.biomaterials.2006.11.042. PubMed PMID: WOS:000244169900011.
[107] Widlund T, Yang S, Hsu Y-Y, Lu N. Stretchability and compliance of freestanding serpentine-shaped ribbons. Int J Solids Struct 2014;51(23–24):4026–37. http://dx.doi.org/10.1016/j.ijsolstr.2014.07.025.
[108] Su YW, Wu J, Fan ZC, Hwang KC, Song JZ, Huang YG, et al. Postbuckling analysis and its application to stretchable electronics. J Mech Phys Solids 2012;60(3):487–508. http://dx.doi.org/10.1016/j.jmps.2011.11.006. PubMed PMID: WOS:000300651900007.
[109] Zhang YH, Xu S, Fu HR, Lee J, Su J, Hwang KC, et al. Buckling in serpentine microstructures and applications in elastomer-supported ultra-stretchable electronics with high areal coverage. Soft Matter 2013;9(33):8062–70. http://dx.doi.org/10.1039/C3sm51360b. PubMed PMID: WOS:000322544200025.
[110] Zhang Y, Fu H, Su Y, Xu S, Cheng H, Fan JA, et al. Mechanics of ultra-stretchable self-similar serpentine interconnects. Acta Mater 2013;61(20):7816–27. doi: http://dx.doi.org/10.1016/j.actamat.2013.09.020.
[111] Fan JA, Yeo WH, Su YW, Hattori Y, Lee W, Jung SY, et al. Fractal design concepts for stretchable electronics. Nat Commun 2014:5. http://dx.doi.org/10.1038/Ncomms426. doi: Artn 3266 PubMed PMID: WOS:000332667600013.
[112] Zhang Y, Fu H, Xu S, Fan JA, Hwang K-C, Jiang J, et al. A hierarchical computational model for stretchable interconnects with fractal-inspired designs. J Mech Phys Solids 2014;72:115–30. doi: http://dx.doi.org/10.1016/j.jmps.2014.07.011.
[113] Hsu YY, Gonzalez M, Bossuyt F, Axisa F, Vanfleteren J, DeWolf I. The effect of pitch on deformation behavior and the stretching-induced failure of a polymer-encapsulated stretchable circuit. J Micromech Microeng 2010;20(7). http://dx.doi.org/10.1088/0960-1317/20/7/07503. doi: Artn 075036. PubMed PMID: WOS:000279260400036.
[114] Hsu YY, Gonzalez M, Bossuyt F, Axisa F, Vanfleteren J, Vandevelde B, et al. Design and analysis of a novel fine pitch and highly stretchable interconnect. Microelectron Int 2010;27(1):33–8. http://dx.doi.org/10.1108/13565361011009504. PubMed PMID: WOS:000274510300006.
[115] Gonzalez M, Vandevelde B, Christiaens W, Hsu YY, Iker F, Bossuyt F, et al. Design and implementation of flexible and stretchable systems. Microelectron Reliab 2011;51(6):1069–76. http://dx.doi.org/10.1016/j.microrel.2011.03.012. PubMed PMID: WOS:000291456600007.
[116] Yang S, Su B, Bitar G, Lu N. Stretchability of indium tin oxide (ITO) serpentine thin films supported by Kapton substrates. Int J Fracture 2014;190(1–2):99–110.
[117] Betz U, Olsson MK, Marthy J, Escola MF, Atamny F. Thin films engineering of indium tin oxide: large area flat panel displays application. Surf Coat Technol 2006;200(20–21):5751–9. http://dx.doi.org/10.1016/j.surfcoat.2005.08.144. PubMed PMID: WOS:000237367600011.
[118] Schmidt H, Flugge H, Winkler T, Bulow T, Riedl T, Kowalsky W. Efficient semitransparent inverted organic solar cells with indium tin oxide top electrode. Appl Phys Lett 2009;94(24). http://dx.doi.org/10.1063/1.315455. doi: Artn 243302. PubMed PMID: WOS:000267166600077.
[119] Leterrier Y, Medico L, Demarco F, Manson JAE, Betz U, Escola MF, et al. Mechanical integrity of transparent conductive oxide films for flexible polymer-based displays. Thin Solid Films 2004;460(1–2):156–66. http://dx.doi.org/10.1016/j.tsf.2004.01.052. PubMed PMID: WOS:000222217500023.
[120] Niu RM, Liu G, Wang C, Zhang G, Ding XD, Sun J. Thickness dependent critical strain in submicron Cu films adherent to polymer substrate. Appl Phys Lett 2007;90(16). doi: Artn 161907 PubMed PMID: WOS:000245870400038.